Characterization of Electrical Interferences for Ground Reaction Sensor Cluster

Qingbo Guo[1], Michael A. Suster[1,2], Rajesh Surapaneni[1], Carlos H. Mastrangelo[1] and Darrin J. Young[1]

[1]Electrical and Computer Engineering Department
The University of Utah
Salt Lake City, Utah, USA
qingbo.guo@utah.edu

[2]EECS Department
Case Western Reserve University
Cleveland, Ohio, USA

Abstract— **This paper presents the characterization of electrical interferences for a high-resolution error-correcting biomechanical ground reaction sensor cluster (GRSC), developed for improving inertial measurement unit (IMU) position sensing accuracy. The GRSC is composed of 13 x 13 sensing nodes, which can measure dynamic ground forces, shear strains, and sole deformation associated with a ground locomotion gait. The integrated sensing electronics consist of a front-end multiplexer that can sequentially connect individual sensing nodes in a GRSC to a capacitance-to-voltage converter followed by an ADC, digital control unit, and driving circuitry to interrogate the GRSC. The characterization data shows that the single-ended (z-axis pressure) mode exhibits a large output interference due to the un-matched interconnect traces design, thus limiting sensing resolution to 8 bits. The differential mode (x/y-axes shear strain) shows a reduced interference effect, achieving a 10-bit resolution.**

I. Introduction

It is highly desirable to track a person's physical location in a GPS-denied environment, for example a fire fighter in a rescue mission, a traveler in a remote area, or a soldier in a battlefield. Commercially available inertial measurement units (IMUs) have been explored for such applications. However, these IMUs exhibit an excessive output drift over time, thus unsuitable for determining an accurate position. It was recently demonstrated that a personal navigation system can be achieved by employing a high-resolution-gait-corrected IMU [1]. The system combines a commercial off-the-shelf (COTS) IMU with a thin and flexible error-correcting biomechanical ground reaction sensor cluster (GRSC). The IMU and GRSC are placed within the heel and at the sole of a personnel boot, as shown in Figure 1, and can be wirelessly connected to a handheld unit that processes inertial and GRSC data in real time. In this approach the IMU can measure inertial displacements while the biomechanical GRSC can independently measure dynamic ground forces, shear strains, and sole deformation associated with a ground locomotion gait. In human bipedal locomotion, the walking mode or gait consists of two separate phases as depicted in Figure 2 [2]. In the swing phase, the leg is off the ground. This period extends from the instant the toe leaves the ground until the heel strikes. In the stance phase, the foot heel first contacts the ground, then it rolls until the midstance is reached, resulting in pivoting of the leg on the ankle and corresponding forward motion of the body. Beyond midstance, detachment of the foot takes place through a gradual rolling. It is evident that only during a fraction of the midstance the velocity of the heel is zero [3]. Pressure sensors array can be employed to detect pressure contours that are generated by the heel if the array is placed between the heel and insole of a shoe. The pressure contours or contours centroid movement as depicted in Figure 3 can calculate periods of zero velocity accurately during the stance phase in a human bipedal locomotion. The zero velocity points in turn can provide discrete zero velocity corrections to the IMU, thus dramatically increasing the positioning accuracy.

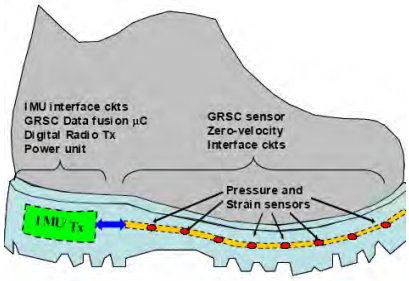

Figure 1. IMU and GRSC embedded personal boot.

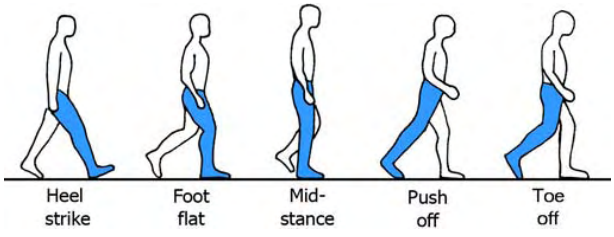

Figure 2. Stance phase in human bipedal locomotion.

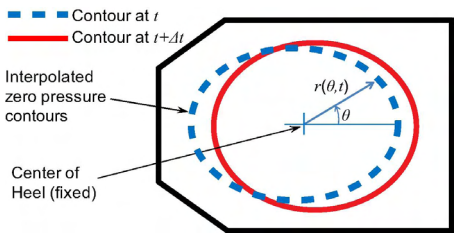

Figure 3. Pressure contours movement during stance phase.

This project has been sponsored under DARPA contract W31P4Q-08-C-0253.

978-1-4577-1767-3/12/$26.00 ©2012 IEEE

Step-corrected (also known as dead reckoning) IMU and GPS navigation systems have been in existence [4-7]. However, these systems detect the step impact shock by employing accelerometers placed away from the ground. This approximate detection technique typically results in a large positioning error, around 1-2% of the distance traveled. In our proposed architecture, a data-rich high-resolution GRSC is placed close to the point of heel to ground contact, thus providing detailed contact information to an IMU located in a close proximity to the GRSC. This extra information and the close mechanical (near rigid) relation between the velocity at the GRSC and IMU location are the key to achieve a highly accurate positioning performance [8]. To verify the concept, a prototype boot incorporating a commercial insole-shaped pressure sensor array was built with an IMU mounted externally to the boot near the heal. The pressure sensors array consists of 99 sensing elements, where 54 elements are located in the heel portion [9]. A loop-closing ½ hour walk test was performed by using the prototypte boot with the nessary signal conditioning and processing algorithms [1]. The field test demonstrated a position error less than 4 meters [1]. To maintain the positioning accuracy for an extended walking time, for example a number of hours for demanding applications, a GRSC with an increased density is required. More data points available from a high-density array are expected to detect much smaller changes during the stationary contact of the heel, thus significantly reducing errors in the zero-velocity calculation during the stance phase. As the GRSC sensing resolution and accuracy increase, low-noise and low-interference sensing electronics become highly critical to accurately capture real-time dynamic response from a ground locomotion gait. An optimized electronic system design and thorough characterization are crucial to minimize environment noise and interference coupling due to the complex system wiring assembly and dynamic movement.

II. Interface Electronic System For Ground Reaction Sensor Cluster

Figure 4 presents the interface electronic system design architecture, consisting of a front-end multiplexer that can sequentially connect 169 individual sensing nodes in a 13 x 13 GRSC to a capacitance-to-voltage (C/V) converter followed by a 12-bit ADC, digital control unit, and driving circuitry. Each GRSC sensing node can be accessed by the corresponding row and column connections. For navigation, pressure sensing along the vertical axis (z-axis) alone is insufficient as the GRSC must be capable of detecting shear force for determining slippage and shoe rotation estimation. Therefore, a combined PDMS-based capacitive pressure and shear strain sensing scheme, consisting of a quad-cell sensing capacitors arrangement that is sensitive to both normal pressure and shear strain, is incorporated inside each sensing node [10, 11]. The z-axis pressure measurement is achieved through the deformation of the PDMS dielectric layer. The shear strain along x and y-axes is detected by the sensing capacitors overlapping area change in a differential manner.

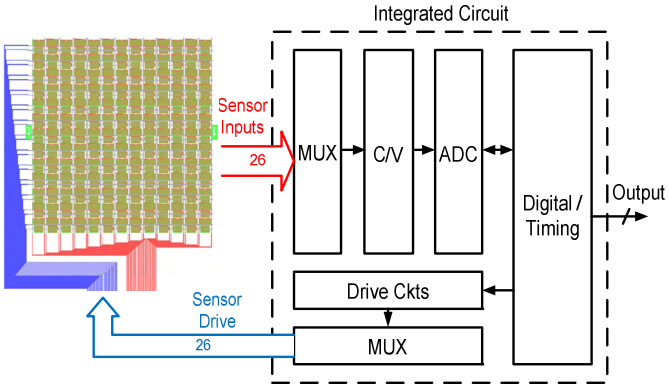

Figure 4. GRSC interface electronic system architecture.

Each sensing node exhibits an area of approximately 2 mm x 2 mm, a nominal capacitance of 0.8 pF/1.6 pF for different modes, and a maximum capacitance change of approximately 10% for the pressure and shear strain sensing, respectively. An electrical model of a GRSC sensing node is presented in Figure 5, where the sensor terminals can be dynamically reconfigured by switches to achieve differential (x/y-axes) shear strain sensing and single-ended (z-axis) vertical pressure sensing.

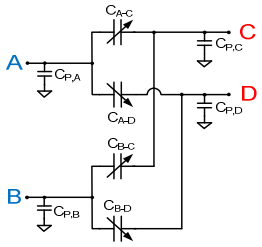

Figure 5. Electrical model of a sensing node in GRSC.

The capacitive sensors are interfaced with a charge amplifier as shown in Figure 6.

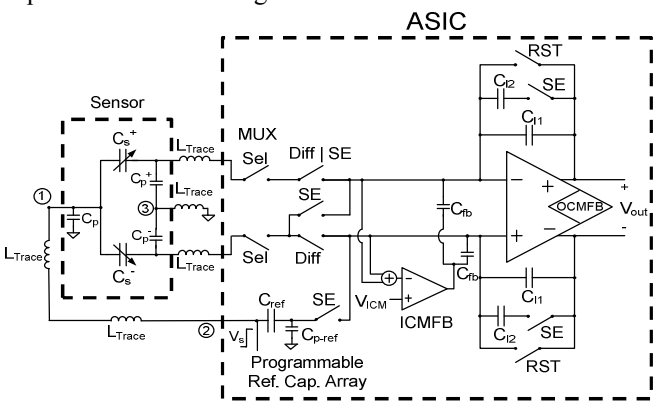

Figure 6. Front-end interface charge amplifier for GRSC.

Different switching schemes are designed for pressure and shear strain sensing. A simulation drive voltage, V_s, is

applied to the sensor to convert the sensor capacitance difference to an output voltage, V_{out}. Input common-mode feedback circuit is incorporated to ensure a proper sensing operation in the presence of amplifier input parasitic capacitance, C_p^+ and C_P^- (mainly composed of capacitances from un-selected sensing nodes) and $C_{P\text{-}ref}$. The single-ended z-axis pressure sensing calls for an on-chip programmable reference capacitor array, C_{ref}, to ensure a close match with the sensor capacitance value, thus suppressing amplifier output offset voltage. In this application, the PDMS-based GRSC is connected to an interface ASIC through relatively long metal traces, which introduce inductances modeled as L_{trace} shown in Figure 5. The inductances can couple the system clock edge transitions to various locations as interference signals, for example (1) drive line interference between nodes 1 and 2, (2) ground interference at node 3, and (3) interference between the amplifier +/- input terminals. These interference signals can contribute to output signal uncertainty, which ultimately limits the system performance.

III. ELECTRICAL INTERFERENCES CHARACTERIZATION

The electronics were designed and fabricated in a 0.35 µm CMOS process and dissipate a DC power of 3 mW from a 3V supply. Characterization of electrical interferences from the three aforementioned sources was thoroughly performed. To characterize the interference on the drive line between nodes 1 and 2, a testing configuration shown in Figure 7 is employed, where a discrete capacitor is used to emulate the sensor capacitance, C_s, with respect to an on-chip programmable reference capacitor, C_{ref}.

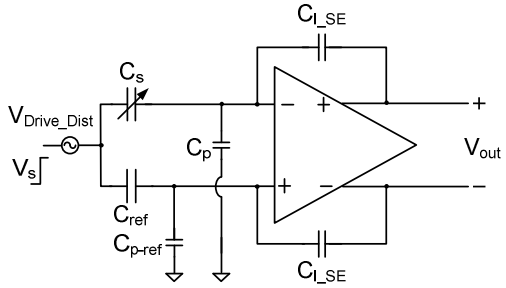

Figure 7. Test configuration for characterizing drive line interference.

The drive line interference, V_{Drive_Dist}, gets amplified to V_{out} by the relationship shown in Equation (1),

$$V_{Out\_Dist} = F\frac{C_s - C_{ref}}{C_{I\_SE}}V_{Drive\_Dist}, \qquad (1)$$

where F is the amplifier filtering factor, which is around 0.1 for the prototype design. It should be noted that this test configuration is viable for the single-ended (z-axis) mode due to a well-controlled programmable C_{ref}. Figure 8 presents the measured output disturbance RMS value as a function of the capacitance difference between C_s and C_{ref} defined as ΔC_z. As ΔC_z increases by 0.3pF, the output disturbance is enhanced by 1.5mV, thus indicating a drive line interference of approximately 24mV.

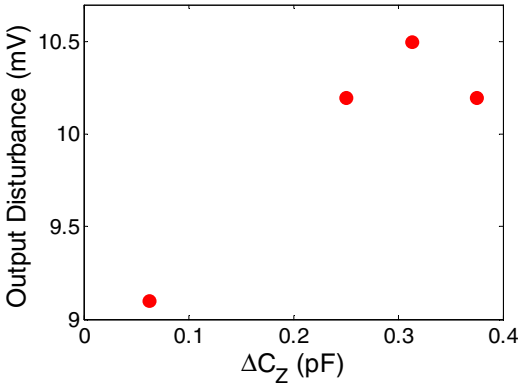

Figure 8. Drive line interference characterization plot.

Figure 9 presents the testing configurations to characterize the ground interference at node 3 for the differential (x/y-axes) and single-ended (z-axis) modes.

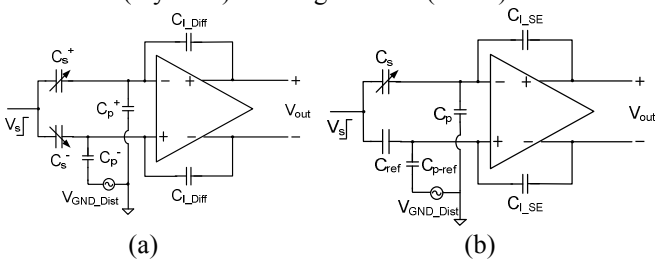

Figure 9. Test configurations for characterizing ground interference: (a) x/y-axes and (b) z-axis.

The ground interference, V_{GND_Dist}, gets amplified to V_{out} by the relationship shown in Equation (2),

$$V_{Out\_Dist} = F\frac{\Delta C_p}{C_I}V_{GND\_Dist}, \qquad (2)$$

where ΔC_p is the difference between the parasitic capacitances at the input of the amplifier, C_I is the amplifier integrating capacitor, and F is the amplifier filtering factor.

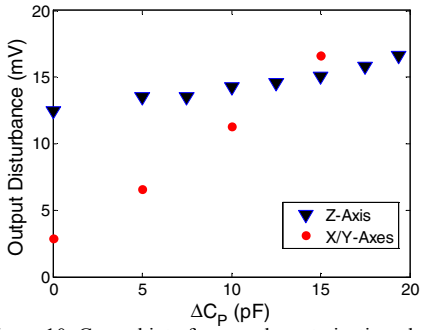

Figure 10. Ground interference characterization plot.

In the differential mode, ΔC_p is obtained by connecting a discrete variable capacitor in parallel to C_p^+, whereas in the single-ended mode it is achieved through programming the $C_{p\text{-}ref}$. Figure 10 shows the measured output disturbance RMS value as a function of ΔC_p for the differential (x/y-

axes) and single-ended (z-axis) modes through interfacing a GRSC with a fabricated interface sensing IC. From the measurement data, the ground interference for both modes can be estimated around 2 mV. It is noted that when ΔC_p is equal to zero, the output interference for the single-ended mode is much larger than that of the differential mode due to other interference signals, which will be described in the following section.

The testing configurations shown in Figure 9 are employed to characterize the interference signals coupled to the amplifier input terminals. Analysis shows that this interference signal gets amplified to V_{out} by the reciprocal of the amplifier feedback factor, which is approximately equal to 50 in the prototype design and is increased with the amplifier input parasitic capacitance. However, the amplifier closed-loop bandwidth is reduced by the same amount in the meantime. Therefore, it is expected that the output interference remains nearly constant as a function of the total input parasitic capacitance. Figure 11 presents the measured output disturbance RMS value as a function of amplifier input parasitic capacitance, revealing the expected behavior.

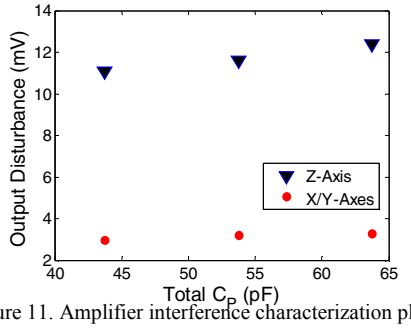

Figure 11. Amplifier interference characterization plot.

It can be seen that the output disturbance in the single-ended mode is much larger than that of the differential mode, corresponding to an amplifier input interference level of 1mV and 0.3mV for the two modes, respectively. The reduced interference in the differential mode is mainly due to a better matched design and layout compared to the single-ended mode. Figure 12 summarizes the effect of different interference signals for the single-ended and differential modes.

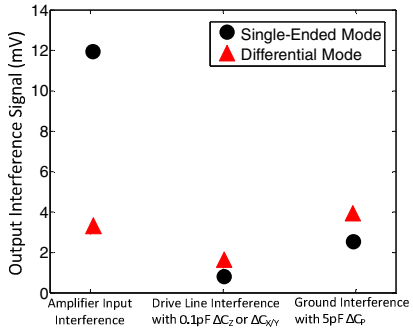

Figure 12. Interference contribution due to different sources.

It is evident that the performance of the single-ended (z-axis) mode is dominantly limited by the amplifier input interference, corresponding to a resolution of 8 bits. In the differential (x/y-axes) mode, all interferences exhibit a comparable effect, achieving a resolution of approximately 10 bits.

IV. Conclusion

A thorough electrical interferences characterization was performed for GRSC. The measurement data shows that the single-ended mode exhibits a large output interference due to the un-matched interconnect traces design, thus limiting sensing resolution to 8 bits. The differential mode shows a reduced interference effect, achieving a 10-bit resolution. Further performance improvements can be expected by employing interferences suppression techniques and better matching for critical wiring traces.

References

[1] O. Bebek, M. A. Suster, S. Rajgopal, M. J. Fu, X. Huang, M. C. Cavusoglu, D. J. Young, M. Mehregany, A. J. van den Bogert, and C. H. Mastrangelo, "Personal Navigation via High-Resolution-Gai-Corrected Inertial Measurement Units," *the IEEE Transactions on Instrumentation and Measurement*, vol. 59, No. 11, pp. 3018–3027, 2010.

[2] M. Trew and T. Everett, *Human movement: an introductory text*, 4th edition, Elsevier Health Sciences, 2001.

[3] H. Lanshammar and L. Strandberg, "Horizontal floor reaction forces and heel movements during the initial stance phase," *Biomechanics VIII-B*, pp. 1123–1128, 1982.

[4] J. Kim, J.-G. Lee, G.-I. Jee, and T. K. Sung, "Compensation of gyroscope errors and gps/dr integration," in *Proc. IEEE Position Location and Navigation Symposium*, April 1996, pp. 464–470.

[5] W.-W. Kao, "Integration of gps and dead reckoning navigation systems," in *Proc. IEEE Vehicle Navigation and Information Systems Conference*, vol. 2, October 1991, pp. 635–643.

[6] E. S. Sazonov, T. Bunpus, S. Zeigler, and S. Marocco, "Classification of plantar pressure and heel acceleration patterns using neural networks," in *Proc. IEEE Neural Networks Conference*, vol. 5, July-August 2005, pp. 3007–3010.

[7] C. Randell, C. Djiallis, and H. Muller, "Personal position measurement using dead reckoning," in *Proc. IEEE International Symposium on Wearable Computers*, October 2005, pp. 166–173.

[8] J. Cheung, M. Zhang, A. Leung, and Y. Fan, "Three-dimensional finite element analysis of the foot during standing-a material sensitivity study," *Journal of Biomechanics*, vol. 38, pp. 1045–1054, 2005.

[9] M. A. Suster, C. H. Mastrangelo, D. J. Young, "Low Power Sensing Electronics for High-Resolution Error-Correcting Biomechanical Ground Reaction Sensor Cluster," *IEEE Sensors Conference*, Hawaii, USA, October 2010, pp. 1020-1023.

[10] R. Surapaneni, K. Park, M. A. Suster, D. J. Young and C. H. Mastrangelo, "A Highly Sensitive Flexible Pressure and Shear Sensor Array for Measurement of Ground Reactions in Pedestrain Navigation," *IEEE Transducers Conference,* June 2011, pp. 906-909.

[11] R. Surapaneni, Y. Xie, Q. Guo, D. Young and C. Mastrangelo, "A High-Resolution Shear and Pressure Imager System Based on Floating Comb Electrodes", the *IEEE Sensors Conference*, Taiwan, R.O.C, 2012.